Harnessing Cobalt-60 Gamma Radiation with ZnTe Gammavoltaic Devices and an LuI_3 Scintillator Interface for Clean Firm Power Generation

Jonah Messinger

Department of Physics and Department of Nuclear, Plasma, and Radiological Engineering
University of Illinois at Urbana-Champaign, Urbana, Illinois, 61801, USA

(Completed May 3, 2021)

Abstract

This study serves as a proof of concept for a gammavoltaic device to harness gamma radiation from cobalt-60 (Co-60). The gammavoltaic device features a high-yield LuI_3 scintillator to absorb gamma radiation and emit ~115,000 low-energy photons per MeV absorbed. The scintillation light illuminates a zinc telluride (ZnTe) photovoltaic cell. The scintillator and an array of photovoltaic cells (surface area of 36 μm^2 per cell) encapsulate a 3.477 cubic centimeter (cm^3) cube of Co-60. The Co-60 gamma radiation power (W m^{-2}) increases as the spatial dimension (m) divided by six, in accordance with the cubic volume to surface area ratio. Crosslight's TCAD software Advanced Physical Models of Semiconductor Devices (APSYS) application is used to simulate the photovoltaic cell performance under various doping and device thickness parameters yielding a maximum photovoltaic cell efficiency of 11.90%. A low-doped photovoltaic cell, which is a more reasonable device to fabricate, was simulated under scintillation illumination from Co-60 gamma radiation at 0, 5, 15, and 20 years from initial decay to demonstrate the longevity of high power output. The proposed gammavoltaic device simulation results in an initial system efficiency of 3.14% and power output of 42,800 (W m^{-2}) and decreases to a system efficiency of 0.98% and power output of 107 (W m^{-2}) after 20 years of operation and no replenishment of the Co-60 gamma radiation source.

I. Introduction & Motivation

Utility-scale clean power generation is a crucial component to global energy decarbonization. Solar photovoltaic (PV) power is a key technology in this regard and produced ~3% of global electricity generation in 2019 [1]. However, solar power is a variable renewable electricity generation resource. Solar PV is fundamentally limited in capacity factor based on terrestrial solar illumination. Capacity factor is a metric that denotes the proportion of annual energy generation to the product of rated power multiplied by the total number of hours in a year. As of 2017, utility-scale solar PV capacity factors in the United States of America (USA) ranged from 14.3% to 35.2% [2]. In short, solar PV only generates electrical power when the sun is shining. Two recent reports detail decarbonization pathways for the USA and both stress the importance of clean firm generation in the power mix, that is, clean power that can operate at high capacity factors approaching 100% [3, 4]. Leveraging similar physics as a PV cell, a gammavoltaic device harnesses gamma-ray radiation from radioactive isotopes for clean, or zero-carbon emission, firm electrical energy generation. Radioactive isotope gamma radiation sources with a long half-life and high specific radiation power can be attractive renewable and zero-carbon energy resources.

Since radioactive isotopes decay, so too gamma radiation power decays. As a result, a gammavoltaic device may require periodic, but potentially infrequent, 'refueling' of the gamma radiation source. However, since the gamma source will decay whether energy is harnessed or not, a gammavoltaic device can be considered a zero-marginal-cost energy resource, similar to traditional variable renewable energy resources. Several radioactive isotope gamma radiation sources have existing and global supply chains, improving the feasibility of the technology. In particular, Cobalt-60 (Co-60) has been synthetically manufactured in nuclear reactors for over 50 years and used in sterilization and the medical sector, and is poised for growth in supply [5-7].

This study is a proof of concept for a novel method to harness gamma radiation for electrical energy conversion, dubbed a 'gammavoltaic' device. In essence, the proposed device will generate a photovoltage, similar to a traditional solar PV cell, from Co-60 gamma radiation. A key difference from traditional solar radiation is that since the proposed gamma radiation is six orders of magnitude greater in energy per incident photon than traditional semiconductor bandgap energy. Therefore, a scintillator material will interface the gamma radiation source and the PV cell. If a reasonably efficient gammavoltaic device can be fabricated in accordance with the simulated device in this study, it presents a significant decarbonization potential for the utility-scale power sector and will merit further experimental study.

II. Technical Background Information

Solid materials with a periodic crystal lattice have electrons that can be characterized by their energy state using band theory and quantum physics. Individual atoms have electron orbitals with discrete energies that have an associated probability density for the position of a given electron equivalent to the square of the electron quantum mechanical wavefunction. The wavefunction, of an electron is described by the time-independent Schrödinger equation and the time-dependent Schrödinger solution, presented in Equation 1 and Equation 2, respectively [8].

$$\frac{-\hbar^2}{2m}\frac{\partial^2 \Psi(x)}{\partial x^2} + V(x)\,\Psi(x) = E\,\Psi(x) \tag{1}$$

$$\psi(x,t) = \Psi(x)\, e^{\frac{-i\,E\,t}{\hbar}} \tag{2}$$

The Pauli exclusion principle forbids two electrons to share the same quantum numbers in a molecule and by extension energy state. Therefore, when atoms join together to form a macro-scale material, such as a crystal lattice, the overlapping atomic orbitals split into two orbitals with different energy levels. At a large number of atoms, the finite energy difference between atomic orbitals approaches zero and hence can be considered to be a band of continuous energy states. Assuming a periodic lattice, these energy states are periodic with respect to the spatial frequency or k-space of a given material. Depending on the number of electrons in a material, these bands can be partially or fully filled. The highest filled energy band occupied with electrons in the ground state is called the valence band and usually consists of bonding orbitals. The lowest unfilled energy band, where at absolute zero temperature, there are no occupied electron states, is called the conduction band and usually consists of antibonding orbitals. Materials with a partially filled valence or conduction band or a conduction band that overlaps in energy with the valence band are generally described as metals and have a high electrical conductivity because they require a negligible electric field to prompt low-energy excitations and drive a current. Whereas, semiconductors and insulators generally have a filled valence band and have energy gaps between the valence and conduction band, known as the bandgap, where no valid energy states exist for electrons to occupy. The bandgap forms at the edge of the k-space periodic range, known as the Brillouin zone. Figure

1 provides a visual illustration of band structure and bandgaps in both spatial and k-space dimensions for metals, semiconductors, and insulators.

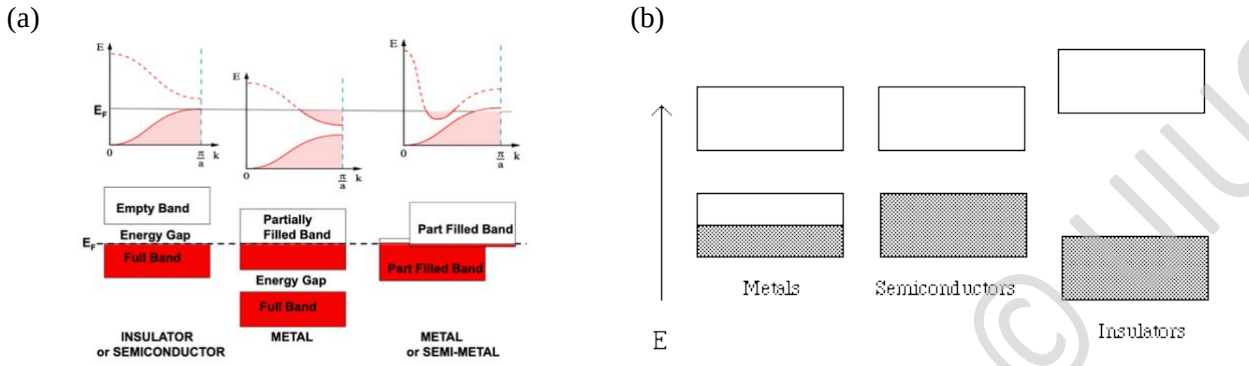

Figure 1: Illustrative band diagrams comparing metals, semiconductors, and insulators in k-space (a) and spatial dimensions (b) [9, 10]

In common practice, the distinction between semiconductors and insulators is a crude and relatively arbitrary cutoff whereby materials with energy gaps greater than 5 electron-volts (eV) are considered to be insulators and lower than 5 eV are considered to be semiconductors. Optical excitations, from photons with energy greater than the bandgap energy, can promote electrons from the valence band to the conduction band allowing these free electron carriers to be conducted as current. Importantly, both photon and phonon particle excitations can only promote one electron to the conduction band per particle and no electron states that satisfy Schrödinger's equation exist in the bandgap, between the valence and conduction bands. Furthermore, semiconductors can be broadly grouped as having a direct or indirect bandgap, which depends on the material band structure. The former requires only optical excitations whereas the latter requires both optical and phonon excitation to free carriers from the valence band.

A. Photovoltaic Device Physics

Band theory and semiconductor physics have given rise to many useful optoelectronic devices for society, which include but are not limited to transistors, diodes, lasers, light emitting diodes, photo-detectors, photovoltaic cells, and more, all of which rely on the concept of a pn-junction. A pn-junction is the joining of a negatively (n) doped and positively (p) doped semiconductor. Electrons from the n-doped region combine with holes in the p-doped region, forming a depletion, or space charge, region, which yields an electric field at the junction. Photovoltaic cells function by extracting optically excited free carriers from conduction band to metal contacts due to the electric field in the depletion region. This process is known as the photovoltaic effect, which is the emergence of a photovoltage, or $V_{\propto}$ in the diagram below, between the effective fermi levels of the p-doped and n-doped regions of the PV cell, upon optical excitation. Figure 2 illustrates the function of a pn-junction in a PV cell.

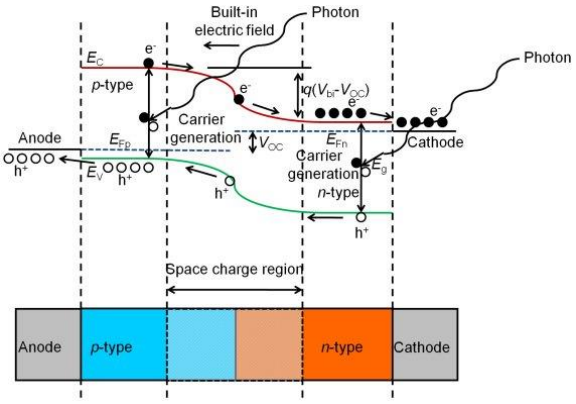

Figure 2: Photovoltaic cell and a pn-junction diagram with incident photons excited free carriers [11]

Photovoltaic cells are characterized by their current and voltage (IV) characteristics, which determine the device short-circuit current (I_{SC}), open circuit voltage (V_{OC}), maximum voltage point (V_{max}), maximum current point (I_{max}), maximum power point (P_{max}), fill factor (FF), and efficiency (η). Equation 3 and Equation 4 define the FF and η in PV cells and Figure 3 provides visual reference for PV cell IV characteristics and device metrics.

$$FF = \frac{V_{max} I_{max}}{V_{OC} I_{SC}} = \frac{P_{max}}{V_{OC} I_{SC}} \tag{3}$$

$$\eta = \frac{V_{OC} I_{SC} FF}{P_{incident}} \tag{4}$$

where $P_{incident}$ is incident optical power

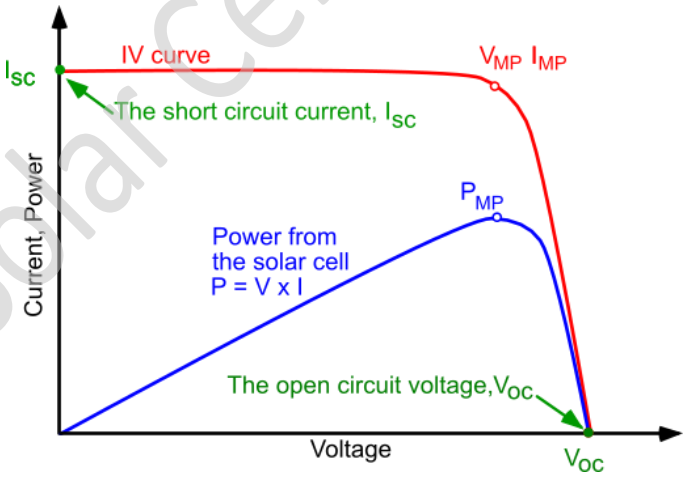

Figure 3: Photovoltaic cell IV Characteristics and maximum power point [12]

B. Gamma Radiation Physics and Cobalt-60 Decay

Radioactive isotopes or nuclides are atoms undergoing nuclear decay due to excess neutrons in the nucleus. Broadly speaking, there are three prominent types of radioactive decay emission: gamma-ray,

beta particle, and alpha particle radiation. Gammy-rays are high energy photons, generally on the order of megaelectronvolts (MeV). Beta particles are high energy emissions on the order of kiloelectronvolts (keV) of either electrons or positrons. Alpha particles are equivalent to helium particles with a two proton and two neutron nucleus. This study will focus on gamma-ray radiation for photonic energy conversion.

Gamma radiation decay for different isotopes varies in the number and energy of gamma ray emissions per decay, the activity of decay, and the half-life. Activity refers to the number of decays per second or a Becquerel (Bq) and half-life is the time for half of a given radioactive material to no longer be radioactive. Specific activity (Bq g^{-1}) is simply the activity of decay per unit mass and similarly, specific radiation power (W g^{-1}) refers to the power of the gamma-ray flux per unit mass. Furthermore, multiplying the density (g cm^{-3}) of a given isotope by its specific power yields radiation power density (W cm^{-3}). These concepts are important in understanding nuclear decay and radiation physics. In selecting a gamma radiation source for a gammavoltaic device, it is important to maximize radiation power density, which corresponds to a high gamma-ray energy emission spectrum and a high specific activity, and to a lesser extent, a high density. However, it is important to note that while a high initial radiation power density is necessary, it not sufficient for a gamma radiation source for a gammavoltaic device, which will need to operate at a reasonably high-power output for years or decades. Therefore, a long half-life, on the order of years, is also desirable to maintain high power output. Very few radiation sources meet these criteria and even fewer have established supply chains. Fortunately, Co-60 is an ideal candidate as it boasts a high gamma-ray energy emission spectrum and decay pathway, as seen in Figure 4, an initial specific activity of 4.1884E13 (Bq g^{-1}), and a half-life of 5.27 years. Initial radiation conditions, such as initial specific activity or initial specific radiation power, of Co-60 refers to the conditions immediately after synthetic manufacture of the isotope, as Co-60 is artificially produced in nuclear reactors by bombarding cobalt-59 or nickel-60 with neutrons [13].

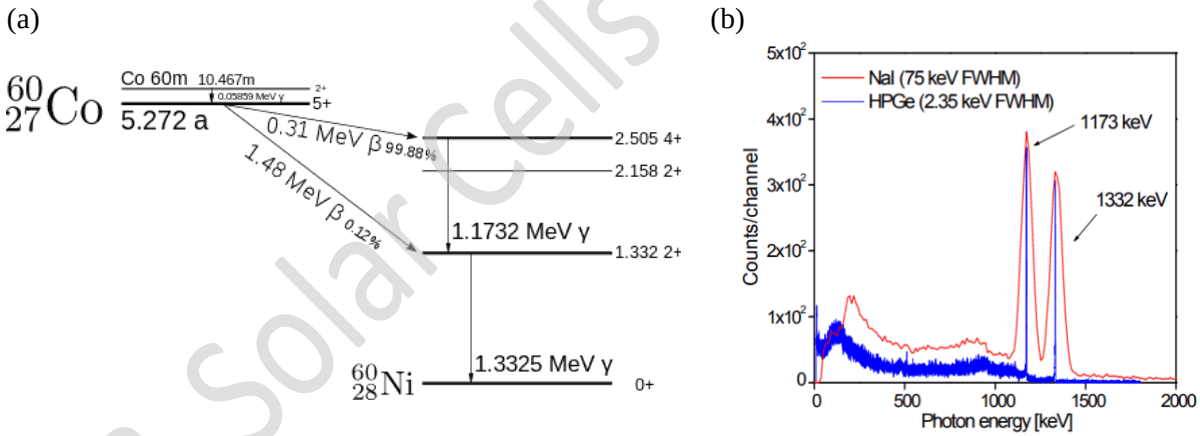

Figure 4: Cobalt-60 nuclear decay pathway diagram (a) and gamma-ray emission spectrum as detected by NaI and HPGe detectors (b) [14]

There are two dominant gamma-ray emissions for Co-60 at 1.1732 MeV and 1.3325 MeV. Equation 5 and Equation 6 detail the temporal exponential decay in both specific activity and radiation power density. Figure 5 compares temporal specific radiation power among four radioactive isotopes and supports the conclusion that Co-60 is indeed an ideal gamma radiation source for gammavoltaic devices. The four isotopes are Co-60, Cesium-134 (Cs-134), Hafnium-178 (Hf-178m2), and Cesium-137 (Cs-137).

$$Specific\ Acitivty = \frac{\ln(2)}{T_{1/2}} \frac{N_{av}}{M_{mol}} e^{-\lambda t} \quad (5)$$

Where $T_{1/2}$ is half-life (s), N_{av} is Avogadro's number, M_{mol} is isotope molar mass, λ is the decay constant equal to $\frac{\ln(2)}{T_{1/2}}$, and t is time since initial decay.

$$\text{Specific Power} = \lambda \frac{N_{av}\, E_\gamma}{M_{mol}}\, e^{-\lambda t} \tag{6}$$

Where E_γ is the total gamma-ray energy emitted per decay.

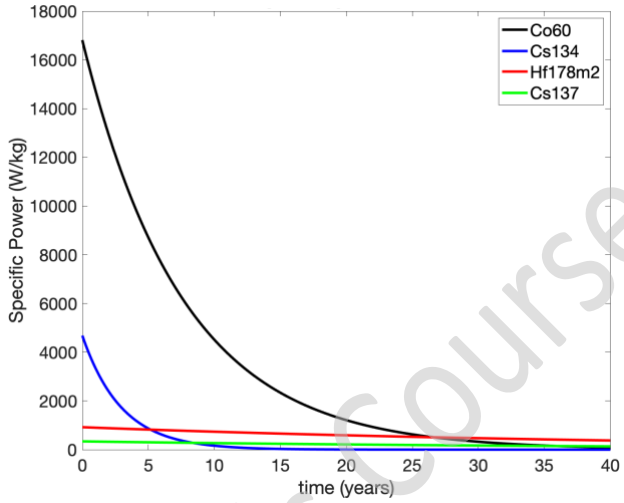

Figure 5: Temporal specific power (W kg^{-1}) for Co-60, Cs-134, Hf178m2, and Cs-137 over 40 years

Scintillation plays a central role in this gammavoltaic device concept. A scintillator is a material that can absorb high energy X-rays or gamma-rays and reemit orders of magnitude more low-energy photons according to a material-specific spectrum. A key parameter for scintillators is yield, also effered to as luminosity, which is defined as the number of low energy photons emitted per 1 MeV of radiation energy absorbed. For radiation with photon energy under 1 MeV, the dominant mechanism for this photomultiplication effect is the photoelectric effect and Compton scattering. The photoelectric effect is similar to the previously described photovoltaic effect with the key difference being the former results in emission of electrons as opposed to the latter, which results in mere excitation of electrons to the conduction band. Compton scattering is a high photon energy process whereby photons scatter off of charged particles such as electrons, and in doing so, impart energy to these charged particles. However, in this study, the Co-60 gamma radiation photon energy exceeds 1 MeV, in which case the dominant scintillation mechanism is dominated by electron positron pair creation [15]. The decay time for the scintillation and photoelectron multiplication process is another crucial parameter in considering scintillator materials. In the context of this study, a decay time on the order of tens of nanoseconds (ns) or less is favorable. In addition, high atomic number materials are favored as it is proportional to the probability of the photoelectric effect occuring [16].

C. State of the Art

The concept of harnessing radiation from radioactive isotope decay for energy conversion is not new. Various devices as well as radiation sources, types, and wavelengths have been proposed in the literature.

Namely, betavoltaic and gammavoltaic devices for the conversion of beta and gamma radiation, respectively, have garnered interest in the research community, mostly for low-power and long-duration applications.

Betavoltaic devices are bombarded by beta particle emission, which in turn generate electron-hole pairs in a pn-junction by impact ionization. Beta particle decay is normally in the keV energy range, roughly three orders of magnitude more energetic than visible photons. These devices are susceptible to radiation damage due to long-term beta particle exposure [17]. In addition, betavoltaic devices often feature extremely low power outputs on the order of nanowatts (nW) or microwatts (μW) [18, 19].

More relevant for this study are Gammavoltaic devices, which are rarer in the literature than betavoltaic devices. Yet, gamma rays are on the order of MeV and potentially more attractive for higher power applications. Several relevant studies on gammavoltaic devices are discussed here. Yoshida et al. investigated a gammavoltaic device, which featured two metal plates with an insulator in-between. The authors performed Monte Carlo N-particle simulations, paired with experimental results, and found a maximum power of 0.093 μW [20]. These devices are markedly different than my proposal, but nevertheless helped inspire my proposed gammavoltaic concept.

Liakos has published extensively on the theory for several gammavoltaic device concepts in a series of research articles. The first publication presents the formalism for a gammavoltaic model for low-energy gamma radiation. Assuming the bandgap energy equals the monochromatic gamma-photon energy, the study finds that the efficiency of the device approaches ~70% with increasing gamma and bandgap energy, and reaches diminishing returns at ~10 eV [21]. Liakos built upon this work taking into account impact ionization and found that impact ionization becomes the dominant photocurrent generation source at ~100 eV gamma-photon energies for a ~3.5 eV bandgap energy semiconductor [22]. Liakos also presents a novel gammavoltaic design with a scintillator interface between a high-energy gamma radiation source, such as Co-60 and a photovoltaic cell. The paper identifies ideal scintillator materials as having a high yield. In this study, monochromatic scintillation emission is assumed, and the optimal design matches the energy of the scintillation light with the bandgap energy of the semiconductor material in the PV cell. However, in reality, even the best scintillator materials have an emission spectrum and scintillation efficiencies around ~30%. Liakos calculates various performance metrics using several different scintillator materials and found that the best scenario was using a Co-60 gamma source, yttrium iodide (doped with cerium) scintillator material, and a semiconductor material with a bandgap energy of 2.26 eV, which yielded an overall device efficiency of 10.42% and maximum power of 832.031 [W m^{-2}] [16]. This proposal for a gamma-ray photovoltaic cell (GRPVC), or as it will be referred to in this study, gammavoltaic, with a scintillator interface is the core inspiration for this study. Glodo et al. has also contributed seminal work on developing high-yield scintillators capable of converting high energy gamma-rays into many low-energy photons on the order of the bandgap energy of many semiconductors used in optoelectronics today [23]. I will build on Liakos' work by taking into account the scintillation spectrum, proposing a specific device structure for further experiential work, proposing a different geometry to allow for higher power output, and advanced simulations, which will be discussed in later sections.

III. Gammavoltaic Design & Device Physics

Solar PV cells harness solar radiation from the sun, which spans a large range of wavelength. Similarly, this study aims to demonstrate the potential for gammavoltaic to harness gamma radiation from radiative isotope sources, which in the case of Co-60 is emitted at two gamma-ray energies. However, these gamma-rays are six orders of magnitude more energetic the bandgap energy for traditional semiconductors. Beyond the mismatch in energy, which would likely result in huge thermalization losses

of excited carriers, absorbing such high energy photons would prove challenging. Hence, this study adopts a scintillator interface concept between the gamma radiation and PV cell, which was described above and in the work of Liakos. [16].

The proposed device is centered around a cube of Co-60, which is wrapped in a thin sheet of aluminum foil, which is assumed to absorb all beta particle emissions, but due to its thin architecture absorbs no gamma-rays. A thin scintillator material is adhered to each surface of the aluminum foil laden Co-60 cube. The scintillator interface absorbs the gamma radiation and emits low-energy photons in accordance with the material specific scintillation light emission spectrum, which illuminates a PV cell. An illustrative diagram of the proposed gammavoltaic device along with the device proposed by Liakos, are shown from a side cross sectional view in Figure 6.

(a) (b)

Figure 6: Illustrative side cross sectional views of the gammavoltaic device proposed in this study (a) and in Liakos (b) [16]

Importantly, each equivalent face of the cube has a significantly higher area than the proposed PV cell. It would be difficult or even impossible to have a microscopic cube of Co-60 manufactured, but more importantly, the incident Co-60 radiation power (W m^{-2}) increases with volume. In particular, it increases linearly as $\frac{d}{6}$, where d is one of the three equivalent spatial dimensions of a cube. This is derived from the fact that the volume (V) of a cube is $V = d^3$ whereas the surface area (SA) of a cube equals $SA = 6 \cdot d^2$. Ultimately, the volume of the proposed cube of Co-60 is somewhat arbitrary but for the purposes of this study, the cube was determined to be 3.477 cubic centimeters (cm^3), where $d = 1.515\ cm$. This volume translates to a radiation power incident to the PV cells, roughly 100 times incident solar power radiation (AM1.5) of 963.56 W m^{-2} and assuming a 36 square micron (μm^2) PV cell surface area, results in 6,375,625 PV cells per face of the cube, an even 2,525 by 2,525 array. Assuming a half-life 0f 5.27 years, calculated initial specific activity of 4.1884E+13 (Bq g^{-1}) from Equation 5, Co-60 density of 8.86 (g cm^{-3}), and a delta function gamma-ray emission spectrum from Co-60 with static corresponding decay probabilities at 346.937 keV (0.00765%), 826.063 keV (0.00768%), 1,173.2374 keV (99.97367%), 1,332.5015 keV (99.98564%), 2,158.5710 keV (0.0011118%), and 2,505 keV (2.0E-64%), the calculated initial power density is 148,957.0719 (kW m^{-3}) [24]. In order to find the incident power (W m^{-2}), the power density must be multiplied by d and divided by six, because each PV cell will only be illuminated from one of six cubic faces. This results in an incident power of 376,116.6066 (W m^{-2}), which when multiplied by the average energy efficiency (27.55%) of the proposed scintillator material, is roughly 100 times that of AM1.5 solar power radiation.

A. Scintillation Spectrum

For this study, LuI_3 will be the scintillation material of choice. Lawrence Berkeley National Laboratory maintains a through database of scintillator materials and associated parameters. LuI_3 has the best combination of high yield at 115,000 [25], high scintillation energy efficiency, low decay time at 28 ns [25], and narrow spectrum, relative to the solar AM1.5 spectrum. Glodo and colleagues were kind enough to share spectrum data for LuI_3 for this study [23]. The spectrum intensity (arbitrary units) was normalized and processed into spectral power density (W m^{-2} μm^{-1}) such that the area under the spectral curve was roughly equivalent to the incident Co-60 radiation power (P_{Co-60}) of 376,116.6066 (W m^{-2}) multiplied by the average scintillation energy efficiency for LuI_3. Equation 7 and Equation 8 elucidate the calculation for wavelength-dependent scintillation energy efficiency (η_s) and spectral power density (P_s), which forms the spectrum used to simulate the illumination of PV cells.

$$\eta_s = \frac{Y\,E_s}{1\,MeV} \tag{7}$$

Where Y is scintillation yield and E_s is the energy equivalent of the spectral wavelength.

$$P_s = P_{Co-60}\,\frac{I_\lambda}{\sum_\lambda I_\lambda}\,\frac{\eta_s}{\lambda_{n+1}-\lambda_n} \tag{8}$$

Where I_λ is normalized intensity at wavelength λ, $\sum_\lambda I_\lambda$ is the sum of all I_λ, and n is the particular data point in the spectrum file, which is associated with a particular wavelength.

Figure 7 shows the spectral power density of the LuI_3 scintillation light spectrum upon gamma-ray absorption from the Co-60 radiation at 0, 5, 10, 15, and 20 years of from initial Co-60 decay, all compared with solar AM1.5 radiation. The temporal dependence of Co-60 radiation is directly related to the theory presented in Equation 5 and Equation 6 and the specific power plot shown in Figure 5.

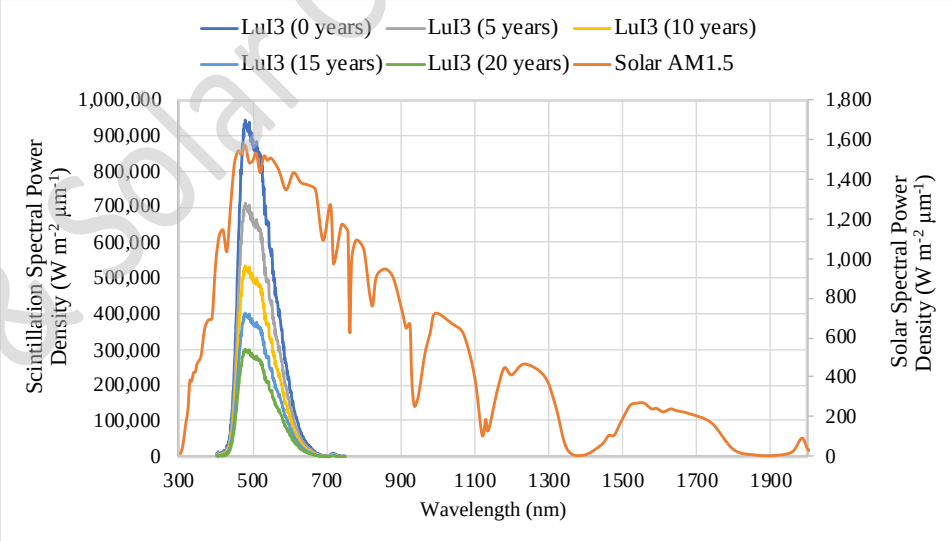

Figure 7: Spectral power density for LuI_3 scintillation of Co-60 gamma radiation at 0, 5, 10, 15, and 20 years after initial decay and solar AM1.5 radiation [23]

B. Selecting ZnTe, Dopants, and Ohmic Contacts

In selecting an appropriate PV cell for the LuI_3 spectrum three key factors were considered: proportion of spectrum available for harnessing, which is dependent on the bandgap energy, a direct bandgap, and relative ease of doping and fabrication or a demonstrated use in solar PV cells in the literature. Zinc Telluride (ZnTe) was the best fit, as most other materials with similar bandgap energy were indirect bandgap semiconductors. With a 2.26 eV direct bandgap, ZnTe is spectrally limited to ~76% of the LuI_3 emission energy. Although n-doping ZnTe can be rather difficult, ZnTe has been used in thin film solar cell devices [26], and is easily p-doped [27]. Nevertheless, recent work has demonstrated effective strategies for n-type doped ZnTe. P-type dopants include copper [28] and arsenic [29], and n-type dopants include aluminum [30], chromium [31], and oxygen [32]. Table 1 enumerates the material properties for ZnTe used in this study and assumed in the device simulation, which will be discussed later. Shallow trap states were incorporated into the simulations, which rely on donor (E_d) and acceptor (E_a) trap energy levels measured from the conduction and valence band, respectively.

Table 1: ZnTe electrical and material properties for simulation

	m_n^*	m_p^*	μ_n	μ_p	E_g	χ	ε	α	E_d	E_a
ZnTe	0.13	0.6	330	80	2.29	3.5	9.67	15,938	19	53.5
Unit	m_0 (kg)	m_0 (kg)	$cm^2\ V^{-1}\ s^{-1}$	$cm^2\ V^{-1}\ s^{-1}$	eV	eV	ε_0 ($C^2\ m^{-2}\ N^{-1}$)	cm^{-1}	meV	meV
Reference	[33]	[33]	[33]	[33]	[33]	[33]	[33, 34]	[34]	[30]	[30]

Ohmic contacts were assumed in the simulation. In highly doped conditions, the necessary work function for ohmic metal contacts on the n-type and p-type region of the ZnTe PV cell can be approximated. In particular, an ohmic metal contact should have a work function approximately less than χ on the n-type side and approximately greater than the sum of E_g and χ on the p-type side. Aluminum ($\Phi = 3.4 - 4.4\ eV$) and platinum ($\Phi = 5.68\ eV$) are good candidates for the n-type and p-type contacts, respectively.

IV. Simulation & Results

The proposed gammavoltaic device was simulated using the Crosslight's TCAD software Advanced Physical Models of Semiconductor Devices (APSYS) application. All simulations were performed assuming a temperature of 300 K. A three-layer ZnTe PV cell was designed and illuminated with the LuI_3 spectrum under initial gamma radiation power conditions. Figure 8 shows the schematic diagram for the model PV cell and a corresponding band diagram under no illumination.

(a) (b)

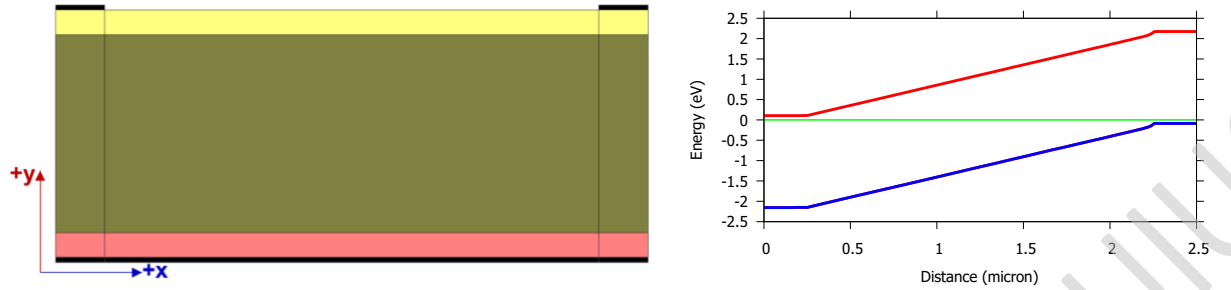

Figure 8: PV cell design schematic with ohmic contacts (a) and corresponding band diagram (b)

The core PV cell design presented in Figure 8 (a) is 6 µm wide and 2.5 µm thick in total. The top ZnTe layer, shown in yellow, is 250 nm n-doped (2E22 m^{-3}), followed by the active middle ZnTe layer, which is 2 µm and slightly p-doped (2E17 m^{-3}), and finally, a 250 nm p-doped (2E23 m^{-3}) ZnTe bottom layer. Table 2 shows 21 iterations of the above design with design parameters and performance metrics reported. The top layer doping (2E25 m^{-3}, 2E24 m^{-3}, and 2E23 m^{-3}), middle layer thickness (1 µm, 2µm, and 3 µm), and middle layer doping (2E19 m^{-3} and 2E21 m^{-3}) were systematically varied over trials 1 through 18 to find optimal design parameters. Trials 19 through 21 attempted to lower doping levels, especially in the n-doped region, to avoid degenerate doping and determine if comparable device efficiencies could be achieved at lower dopant concentrations. Indeed trials 19, 20, and 21 demonstrate that this is possible. Not listed in Table 2 are the top and bottom layer thickness, both of which are kept constant at 250 nm through all trials.

Table 2: Tabulation of PV cell design parameters and simulated device performance metrics by trial

Trial #	Top Layer Thickness (µm)	Top Layer n-type doping (m^-3)	Middle Layer Thickness (µm)	Middle Layer p-type doping (m^-3)	Bottom Layer p-type doping (m^-3)	Voc (V)	Jsc (A m^-2)	Pmax (W m^-2)	Vmax (V)	Jmax (A m^-2)	FF (%)	Device Efficiency (%)
1	0.25	2.00E+25	1	2.00E+19	2.00E+24	1.90	2.54E+04	4.22E+04	1.77	2.38E+04	87.46%	11.22%
2	0.25	2.00E+25	1	2.00E+21	2.00E+24	1.89	2.55E+04	4.30E+04	1.77	2.43E+04	89.28%	11.43%
3	0.25	2.00E+25	2	2.00E+19	2.00E+24	1.85	2.82E+04	4.48E+04	1.62	2.76E+04	85.65%	11.90%
4	0.25	2.00E+25	2	2.00E+21	2.00E+24	1.87	2.75E+04	4.37E+04	1.76	2.49E+04	85.21%	11.62%
5	0.25	2.00E+25	3	2.00E+19	2.00E+24	1.77	2.87E+04	4.44E+04	1.62	2.74E+04	87.17%	11.80%
6	0.25	2.00E+25	3	2.00E+21	2.00E+24	1.77	2.53E+04	3.89E+04	1.76	2.21E+04	86.58%	10.33%
7	0.25	2.00E+24	1	2.00E+19	2.00E+24	1.89	2.55E+04	4.22E+04	1.76	2.40E+04	87.89%	11.23%
8	0.25	2.00E+24	1	2.00E+21	2.00E+24	1.89	2.55E+04	4.28E+04	1.76	2.44E+04	89.00%	11.38%
9	0.25	2.00E+24	2	2.00E+19	2.00E+24	1.87	2.82E+04	4.47E+04	1.62	2.76E+04	84.95%	11.89%
10	0.25	2.00E+24	2	2.00E+21	2.00E+24	1.87	2.75E+04	4.39E+04	1.76	2.50E+04	85.52%	11.67%
11	0.25	2.00E+24	3	2.00E+19	2.00E+24	1.83	2.87E+04	4.43E+04	1.62	2.73E+04	84.44%	11.78%
12	0.25	2.00E+24	3	2.00E+21	2.00E+24	1.84	2.53E+04	3.88E+04	1.74	2.23E+04	83.56%	10.32%
13	0.25	2.00E+23	1	2.00E+19	2.00E+24	1.86	2.55E+04	4.22E+04	1.76	2.40E+04	89.06%	11.21%
14	0.25	2.00E+23	1	2.00E+21	2.00E+24	1.88	2.55E+04	4.27E+04	1.76	2.43E+04	88.82%	11.34%
15	0.25	2.00E+23	2	2.00E+19	2.00E+24	1.76	2.82E+04	4.47E+04	1.62	2.75E+04	89.81%	11.88%
16	0.25	2.00E+23	2	2.00E+21	2.00E+24	1.86	2.74E+04	4.37E+04	1.76	2.49E+04	85.65%	11.63%
17	0.25	2.00E+23	3	2.00E+19	2.00E+24	1.85	2.87E+04	4.42E+04	1.62	2.72E+04	83.28%	11.75%
18	0.25	2.00E+23	3	2.00E+21	2.00E+24	1.84	2.53E+04	3.87E+04	1.74	2.23E+04	83.55%	10.30%
19	0.25	2.00E+22	2	2.00E+17	2.00E+22	1.77	2.84E+04	4.46E+04	1.62	2.75E+04	88.97%	11.86%
20	0.25	2.00E+21	2	2.00E+17	2.00E+21	1.53	2.88E+04	4.13E+04	1.49	2.78E+04	93.78%	10.99%
21	0.25	2.00E+21	2.25	2.00E+17	2.00E+22	1.82	2.86E+04	4.43E+04	1.62	2.73E+04	85.02%	11.79%

It seems the 2 µm thick active layer was ideal, which agrees with the estimation of minority carrier electron diffusion length at 300 K of 2.29 µm. In other words, free electron carriers excited in the active layer should be extracted by the in-built pn-junction electric field and migrate to the n-doped region before recombining with a hole. However, calculations for holes suggested a diffusion length of only 1.438 µm, more than half a micron smaller than the active layer thickness, which appears to disagree with these results. Equation 9 shows the method for estimating diffusion length (L), assuming 10 ns for non-radiative carrier lifetime (τ_{nr}), as per the source code in APSYS, and using parameters listed in Table 1.

$$L_{n/p} = \sqrt{D_{n/p}\,\tau_{nr}} = \sqrt{\frac{\mu_{n/p}\,K_B\,T\,\tau_{nr}}{q}} \tag{9}$$

Where n/p is for electron and holes, respetivley, D is diffusion constant, μ is carrier mobility, K_B is the Boltzmann constant, T is temperature (300 K), and q is the fundamental charge (C) of an electron.

The diffusion length estimation was used as an approximate upper bound for the active middle layer thickness. However, absorption is also an important governing factor in designing the PV cell thickness. As reported in Table 1, the absorption coefficient of ZnTe is found to be 15,938 cm^{-1} [34]. Equation 10 offers a method to estimate the thickness required to absorb 99% of incident photons, which is determined to be ~2.889 μm. Since the optimal thickness from an absorption perspective is greater than the estimated carrier diffusion lengths, there will be a trade-off in thickness where increasing active layer thickness will result in increased photon absorption but also increase recombination. The former is essential for device efficiency while the latter is deleterious. This optimization challenge between absorption and diffusion length helps to explain the inconsistency in the optimal layer thickness being 2 μm, among the variations simulated, despite the hole diffusion length estimation being only 1.438 μm.

$$X = -\ln\left(\frac{I}{I_0}\right)\frac{1}{\alpha} \tag{10}$$

Where X is the required active layer thickness, $\frac{I}{I_0}$ is the proportion of photons not absorbed, and α is absorption coefficient.

Figure 9 plots relative energy density throughout the PV cell and an JV (J is analogous to I in IV where J include area dimensions) characteristics plot to show the V_{OC} and J_{SC} for the best device, which was simulation trial #3. The relative energy density exponential falls to zero through the thickness of the PV cell, which can be explained by absorption of incident photons. This absorption is exponential and as photons are absorbed there is less energy available deeper in the PV cell.

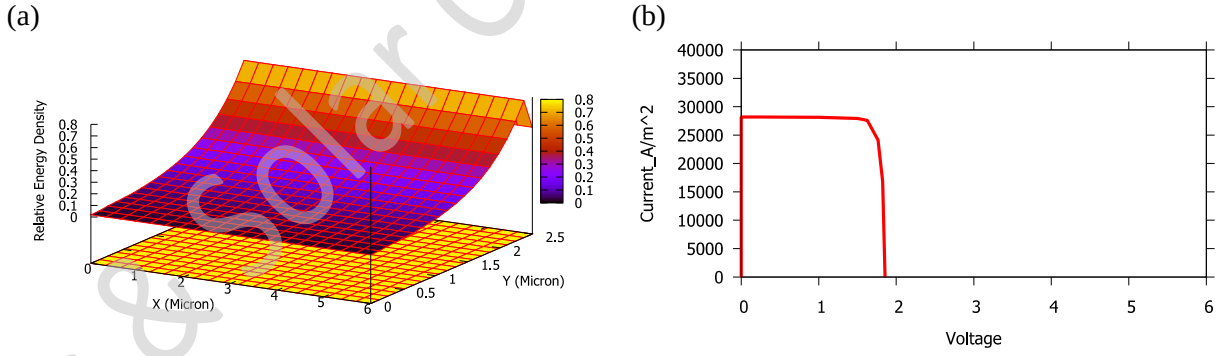

Figure 9: Relative energy density (a) and JV characteristics (b) are reported for the highest performing PV cell design (trial #3)

Overall, the various trials maintain a fairly constant and modest distribution in device efficiency between 10% and 11%. While these efficiencies are respectable, PV cell researchers will be quick to point out that there is room for improvement and in particular potential for improved V_{OC}. Certainly a multijunction design would improve efficiency. However, the most significant metric to demonstrate the efficacy of this gammavoltaic concept is P_{max}. At first glance, most PV cell researchers would assume

these power-per-square-meter figures were reported in error. Nevertheless, these high-power outputs are indeed in correct units. By scaling the volume of the cubic Co-60 gamma radiation source, as described in Section III, the gamma radiation power incident on the LuI_3 scintillator increases linearly. To be clear, this argument is not that the total power through a larger area increases, which is of course obvious, but rather that, in fact, the total power-per-square-meter increases linearly. This results in a high scintillation light intensity, which generates more electron-hole pairs in the PV cell. As a result, remarkably high current and power outputs are achievable for gammavoltaic devices.

The last set of simulations were intended to assess the temporal power outputs for a gammavoltaic device. To be sure, it will decrease exponentially, as shown in Figure 7, however, because the half-life for Co-60 is 5.27 years, the exponential decay constant terms in Equation 5 and Equation 6 are very small at roughly 0.132 $year^{-1}$. In other words, every ~7.6 years the Co-60 gamma radiation will drop ~36.79%. It is assumed in this analysis that this exact exponential decay will directly apply to the scintillation light power as well, although a more rigorous analysis may find that this is not necessarily the case. A temporal evaluation of gammavoltaic power output was performed by simulating a model PV cell illuminated by LuI_3 scintillation light from Co-60 gamma radiation at 0, 5, 10, 15, and 20 years after initial radioactive decay. The model PV cell has lower and more realistic doping concentrations as seen in trials 19, 20, and 21 of Table 2. The model device featured a 250 nm n-doped (2E22 m^{-3}) top ZnTe layer, a 2 µm slightly p-doped (2E17 m^{-3}) middle ZnTe layer, and a 250 nm p-doped (2E23 m^{-3}) bottom ZnTe layer. Figure 10 plots the power output for the above mentioned gammavoltaic device over a 20-year timeframe. Table 3 presents the data in Figure 10 along with other device performance metrics and includes the proposed gammavoltaic device performance under solar AM1.5 illumination as a reference.

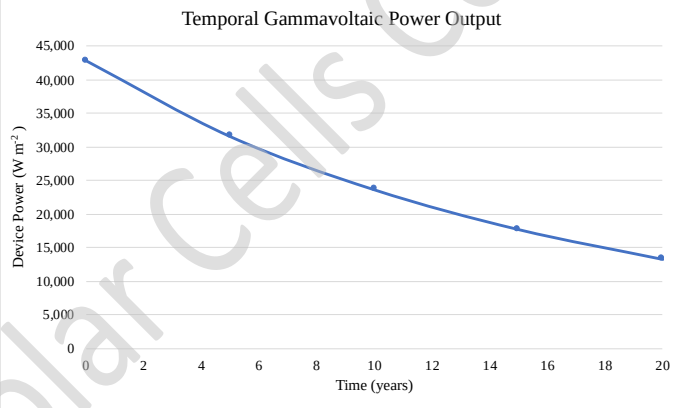

Figure 10: Temporal power output for gammavoltaic device over 20 years

Interestingly, the exponential decay in gammavoltaic device power, shown in Figure 10, has a different decay constant. An exponential fit in Tableau with an r-squared value of 0.99984 resulted in the following relationship, $P_{max} = 42{,}535.7\ e^{-0.058 \cdot t}$, where t is time in years. The decay constant for Co-60 gamma radiation power is -0.132. The exact cause for this phenomenon requires further investigation.

Table 3: Temporal gammavoltaic device performance over 20 years and solar AM1.5 reference

Year	Voc (V)	Jsc (A m^-2)	Pmax (W m^-2)	Vmax (V)	Jmax (A m^-2)	FF (%)	Device Efficiency (%)	Gamma Radiation Power (W m^-2)	Scintillation Spectrum Power (W m^-2)	Scintillation Energy Efficiency (%)	System Efficiency (%)
0	1.83	2.83E+04	4.28E+04	1.74	2.46E+04	82.61%	11.39%	3.76E+05	1.04E+05	27.55%	3.14%
5	1.82	2.13E+04	3.16E+04	1.57	2.01E+04	81.40%	8.39%	2.83E+05	7.79E+04	27.55%	2.31%
10	1.82	1.60E+04	2.37E+04	1.51	1.57E+04	81.37%	6.29%	2.12E+05	5.85E+04	27.55%	1.73%
15	1.78	1.20E+04	1.78E+04	1.51	1.18E+04	82.93%	4.72%	1.60E+05	4.40E+04	27.55%	1.30%
20	1.77	9.03E+03	1.33E+04	1.51	8.85E+03	83.25%	3.54%	1.20E+05	3.31E+04	27.55%	0.98%
AM1.5	1.51	7.82E+01	1.07E+02	1.49	7.19E+01	90.65%	0.03%	N/A	N/A	N/A	N/A

In order to obtain a true system efficiency, the device efficiency is multiplied by the scintillation energy efficiency. This system efficiency characterizes the percentage of gamma radiation power harnessed for electrical power generation and is presented in Table 3. While system efficiency is quite small, the most important metric is power output, which as shown in Figure 10, is remarkably high throughout the 20 year simulation.

V. Summary & Conclusion

This study built off of previous work by Liakos on a proposal for harnessing gamma radiation from Co-60 with a high-yield scintillator and PV cell [16]. LuI_3 was selected as the optimal scintillator because it combined an extremely high yield and scintillation energy efficiency with a short scintillation decay time. The LuI_3 scintillation spectrum was modeled under gamma radiation from a cube of Co-60 and used to illuminate several variations of a single junction ZnTe PV cell. This gammavoltaic device concept was simulated at 0, 5, 10, 15, and 20 years after initial decay to demonstrate the temporal variation in the gammavoltaic cell power output. Further investigations should explore multi-junction PV cells to increase efficiency and assess the thermal management requirements of thermalization in the scintillator and PV cell. A subsequent analysis could assess how often the Co-60 gamma radiation source should be replenished to ensure a more stable power output over several decades. In addition, if it is possible to extract the photoelectrons and excited carriers within the scintillator itself as opposed to scintillating photons to illuminate a PV cell, the efficiency of the overall gammavoltaic device would increase dramatically. The results of this study suggest that gammavoltaics may have potential in utility-scale clean firm power generation.

VI. Acknowledgements

I greatly appreciate the guidance and teaching of Professor Can Bayram of the Electrical and Computer Engineering (ECE) Department and the Micro & Nanotechnology Laboratory. Professor Bayram is the Professor for ECE 443: LEDs & Solar Cells, for which this study was prepared. I would also like to express my sincerest gratitude to the teaching assistants for ECE 443: Marwan Mohamed Eladl, Sanat Pandey, and Yi-Chia Tsai. Marwan was instrumental in teaching me how to use the Crosslight TCAD software and utilize more complex simulation methodologies. Sanat helped me frame my project, specify the important device parameters, and consider various physical and experimental constraints to bolster the proposed device. Yi-Chia helped me learn the theory necessary to be successful in ECE 443 and navigate the various complexities of the Crosslight TCAD software. I would also like to the Dr. Liakos for advising on the gammavoltaic concept and to Dr. Glodo for sharing extremely high quality experiential LuI_3 spectral data.

This project would not have been possible without support from the National Science Foundation, Naval Research Laboratory, IBM, MicroLink Devices, and Crosslight for ECE 443 and the sponsorship of the TCAD software used for all the simulations in this study by Crosslight Inc.

VII. References

[1] IEA, "Solar PV," IEA, 2020. [Online]. Available: https://www.iea.org/reports/solar-pv

[2] B. Mark and S. Joachim, "Utility-Scale Solar: Empirical Trends in Project Technology, Cost, Performance, and PPA Pricing in the United States – 2018 Edition," 2018. [Online]. Available: https://emp.lbl.gov/utility-scale-solar/

[3] C. Clack, "Insights from Modeling the Decarbonization of the United States Economy by 2050," in "Deep Decarbonization Initiative," Vibrant Clean Energy, University of California San Diego, Virtual Meeting, January 27, 2021. https://vibrantcleanenergy.com/wp-content/uploads/2021/01/VCE-UCSD-01272021.pdf

[4] C. G. E. Larson, J. Jenkins, E. Mayfield, A. Pascale, C. Zhang, J. Drossman, R. Williams, S. Pacala, R. Socolow, EJ Baik, R. Birdsey, R. Duke, R. Jones, B. Haley, E. Leslie, K. Paustian, and A. Swan, "Net-Zero America: Potential Pathways, Infrastructure, and Impacts," Princeton University, interim report, December 15, 2020. [Online]. Available: https://environmenthalfcentury.princeton.edu/sites/g/files/toruqf331/files/2020-12/Princeton_NZA_Interim_Report_15_Dec_2020_FINAL.pdf

[5] R. A. Wiens, *Ensuring a reliable global Cobalt-60 supply for the next generation*. India: National Association for Applications of Radioisotopes and Radiation in Industry, 2018. https://naarri.com/images/day%2001/IT7%20Richard%20Wiens%20-%20Ensuring%20a%20reliable%20global%20Cobalt-60%20supply%20for%20the%20next%20generation-min.pdf

[6] "Nordion Acquires Technology to Expand Future Global Cobalt-60 Supply," ed: Nordion, a Sotera Health company, 2019. https://www.newswire.ca/news-releases/nordion-acquires-technology-to-expand-future-global-cobalt-60-supply-861305527.html

[7] "The Source. The Standard. C-188 COBALT-60," ed: MDS Nordion Inc., 2001. https://www.nrc.gov/docs/ML1033/ML103370379.pdf

[8] D. J. Griffiths, *Introduction to Quantum Mechanics*, 3rd ed. Cambridge: Cambridge University Press, 2018. https://www.cambridge.org/core/books/introduction-to-quantum-mechanics/990799CA07A83FC5312402AF6860311E

[9] "Solid State Theory Physics 545: Band Theory III." Bilkent University. http://www.fen.bilkent.edu.tr/~gulseren/phys545/pdf/bands3.pdf (accessed April 25, 2021).

[10] "Scientific Principles: Conductors, Insulators, and Semiconductors." Department of Materials Science and Engineering, University of Illinois at Urbana-Champaign. http://matse1.matse.illinois.edu/sc/prin.html (accessed April 25, 2021).

[11] M. Shanawani, D. Masotti, and A. Costanzo, "THz Rectennas and Their Design Rules," *Electronics*, vol. 6, no. 4, p. 99, 2017. [Online]. Available: https://www.mdpi.com/2079-9292/6/4/99.

[12] "Solar Cell Parameters: IV Curve." PV Education. https://www.pveducation.org/pvcdrom/solar-cell-operation/iv-curve (accessed May 2, 2021).

[13] (2002). *Cobalt-60 (60Co) Fact Sheet*. [Online] Available: https://www.doh.wa.gov/portals/1/Documents/Pubs/320-078_co60_fs.pdf

[14] "Cobalt-60 Spectrum." Nuclear Power for Everybody. https://www.nuclear-power.net/nuclear-engineering/radiation-detection/gamma-spectroscopy/cobalt-60-spectrum/ (accessed May 2, 2021).

[15] R. S. Feigelson. "What are scintillator materials?" Scintillator Materials Group, Stanford University. https://web.stanford.edu/group/scintillators/scintillators.html (accessed May 3, 2021).

[16] J. K. Liakos, "Gamma-ray-driven photovoltaic cells via a scintillator interface," *Journal of Nuclear Science and Technology (Tokyo)*, vol. 48, no. 12, pp. 1428-1436, 2011. [Online]. Available: http://inis.iaea.org/search/search.aspx?orig_q=RN:43055355.

[17] S. Harrison. S. University. (2013). Betavoltaic Devices. Available: http://large.stanford.edu/courses/2013/ph241/harrison2/

[18] T. Shimaoka, H. Umezawa, K. Ichikawa, J. Pernot, and S. Koizumi, "Ultrahigh conversion efficiency of betavoltaic cell using diamond pn junction," *Applied Physics Letters*, vol. 117, no. 10, p. 103902, 2020, doi: 10.1063/5.0020135. https://aip.scitation.org/doi/abs/10.1063/5.0020135
[19] C. Delfaure, M. Pomorski, J. d. Sanoit, P. Bergonzo, and S. Saada, "Single crystal CVD diamond membranes for betavoltaic cells," *Applied Physics Letters*, vol. 108, no. 25, p. 252105, 2016, doi: 10.1063/1.4954013. https://aip.scitation.org/doi/abs/10.1063/1.4954013
[20] T. Yoshida, A. Y. K. Chen, J. Nozawa, N. Sugie, and T. Tanabe, "An Attempt to Directly Convert Gamma-Ray Energy into Electricity," *Nuclear Science and Engineering*, vol. 150, no. 3, pp. 362-367, 2005/07/01 2005, doi: 10.13182/NSE05-A2523. https://doi.org/10.13182/NSE05-A2523
[21] J. K. Liakos, "Gamma ray driven photovoltaic cells: an interface between nuclear and semiconductor physics," *Semiconductor Science and Technology*, vol. 23, no. 8, p. 085001, 2008/06/10 2008, doi: 10.1088/0268-1242/23/8/085001. http://dx.doi.org/10.1088/0268-1242/23/8/085001
[22] J. K. Liakos, "Effect of B–B impact ionization on GRPVC output: a semiconductor–nuclear physics interface," *Journal of Physics D: Applied Physics*, vol. 42, no. 13, p. 135105, 2009/06/11 2009, doi: 10.1088/0022-3727/42/13/135105. http://dx.doi.org/10.1088/0022-3727/42/13/135105
[23] J. Glodo, E. V. D. v. Loef, W. M. Higgins, and K. S. Shah, "Mixed Lutetium Iodide Compounds," *IEEE Transactions on Nuclear Science*, vol. 55, no. 3, pp. 1496-1500, 2008, doi: 10.1109/TNS.2008.922215. https://ieeexplore-ieee-org.proxy2.library.illinois.edu/document/4545125/figures#figures
[24] "WWW Table of Radioactive Isotopes." LUNDS UNIVERSITET. http://nucleardata.nuclear.lu.se/toi/nuclide.asp?iZA=270060 (accessed May 2, 2021).
[25] M. B. S. Derenzo, M. Weber, and K. Brennan. "Scintillation Properties." Lawrence Berkeley National Laboratory. http://scintillator.lbl.gov (accessed May 2, 2021).
[26] T. Tanaka *et al.*, "Demonstration of homojunction ZnTe solar cells," *Journal of Applied Physics*, vol. 108, no. 2, p. 024502, 2010, doi: 10.1063/1.3463421. https://aip.scitation.org/doi/abs/10.1063/1.3463421
[27] J. D. Dow *et al.*, "Proposed explanation of the p-type doping proclivity of ZnTe," *Physical Review B*, vol. 43, no. 5, pp. 4396-4407, 02/15/ 1991, doi: 10.1103/PhysRevB.43.4396. https://link.aps.org/doi/10.1103/PhysRevB.43.4396
[28] W. Mahmood *et al.*, "Pronounced Impact of p-Type Carriers and Reduction of Bandgap in Semiconducting ZnTe Thin Films by Cu Doping for Intermediate Buffer Layer in Heterojunction Solar Cells," (in eng), *Materials (Basel)*, vol. 12, no. 8, p. 1359, 2019, doi: 10.3390/ma12081359. https://pubmed.ncbi.nlm.nih.gov/31027289
[29] F. S. Turco-Sandroff, M. J. S. P. Brasil, R. E. Nahory, R. J. Martin, Y. Zhang, and B. J. Skromme, "Arsenic-doped P-type ZnTe grown by molecular beam epitaxy," *Applied Physics Letters*, vol. 59, no. 6, pp. 688-690, 1991, doi: 10.1063/1.105366. https://aip.scitation.org/doi/abs/10.1063/1.105366
[30] K. Saito, T. Saeki, X. Han, T. Tanaka, Q. Guo, and M. Nishio, *Estimation of donor and acceptor levels in Al-doped ZnTe layers from photoluminescence measurement* (Seventh International Conference on Thin Film Physics and Applications). SPIE, 2011. https://doi.org/10.1117/12.888520
[31] P. Singh and A. Mookerjee, "Effect of donor (I) or acceptor (N) co-doping on Cr doped (ZnTe)12 clusters," *Journal of Magnetism and Magnetic Materials*, vol. 323, no. 1, pp. 166-174, 2011/01/01/ 2011, doi: https://doi.org/10.1016/j.jmmm.2010.08.058.
[32] C. Tablero, "Acceptor and donor ionization energy levels in O-doped ZnTe," *Computational Materials Science*, vol. 49, no. 2, pp. 368-371, 2010/08/01/ 2010, doi: https://doi.org/10.1016/j.commatsci.2010.05.023.
[33] N. Amin, K. Sopian, and M. Konagai, "Numerical modeling of CdS/CdTe and CdS/CdTe/ZnTe solar cells as a function of CdTe thickness," *Solar Energy Materials and Solar Cells*, vol. 91, no. 13, pp. 1202-1208, 2007/08/15/ 2007, doi: https://doi.org/10.1016/j.solmat.2007.04.006.
[34] K. Sato and S. Adachi, "Optical properties of ZnTe," *Journal of Applied Physics*, vol. 73, no. 2, pp. 926-931, 1993, doi: 10.1063/1.353305. https://aip.scitation.org/doi/abs/10.1063/1.353305